Ultrasonics Sonochemistry 87 (2022) 106034

Contents lists available at ScienceDirect

Ultrasonics Sonochemistry

journal homepage: www.elsevier.com/locate/ultson

Influence of rigid wall on the nonlinear pulsation of nearby bubble

Xun Wang [a], Weizhong Chen [b,*], Min Zhou [c], Zekun Zhang [a], Lingling Zhang [b]

[a] Kaiserslautern Intelligent Manufacturing School, Shanghai Dianji University, Shanghai 201306, China
[b] Key Laboratory of Modern Acoustics, Ministry of Education, Institute of Acoustics, Nanjing University, Nanjing 210093, China
[c] School of Science, Xi'an Polytechnic University, Xi'an 710048, China

ARTICLE INFO

Keywords:
Bubble dynamics
Nonlinear pulsation
Rigid wall
Bifurcation diagram

ABSTRACT

This paper mainly focuses on the nonlinear pulsation of a bubble near the rigid wall. Dynamics of near-wall bubble and free bubble are discussed and compared in details. Investigation reveals as the driving acoustic pressure amplitude increases, nonlinear pulsation of bubble becomes intense gradually. Besides, decreasing the viscosity of host liquid is advantageous for the nonlinear pulsation of bubble. Bifurcation diagrams of bubble radius show acoustic reflection of the rigid wall makes the initial bifurcation appear at low driving acoustic amplitude and on bubble with small ambient radius, and makes the bifurcation still exist for bubble in high-viscosity liquids. That indicates the rigid wall will produce enhancement on the nonlinearity of nearby bubble. As the bubble approaches the wall, the enhancement becomes strong. Moreover, research on the influence of driving frequency shows the rigid wall makes the frequency band corresponding to chaos around the resonant frequency of free bubble shift downward.

1. Introduction

Irradiation of ultrasound wave with enough amplitude into liquid makes the gas nuclei grow to visible bubbles. This phenomenon is named as ultrasonic cavitation [1–4]. When the bubbles collapse, high temperature is generated in them and enormous energy is released to the surrounding liquid [5]. Cavitation has been widely used in all kinds of fields, such as sonochemistry [6–8], cleaning [9,10], emulsification [11] and so on. If the amplitude of driving pressure is high enough, nonlinear pulsation of bubble will emerge [12,13]. Investigating the nonlinearity of bubble pulsation is advantageous for the application of cavitation.

There are a considerable number of publications study the nonlinear properties of pulsating bubbles. Sojahrood et al. [14] discussed the super-harmonic and ultra-harmonic behavior of the acoustically excited bubble. Not only the conventional bifurcation analysis but also the maxima analysis are used to evaluate the bubble dynamics. Results show combining these two methods is helpful for having a comprehensive knowledge about the bubble pulsation. Besides, they investigated the nonlinear behavior of the microbubbles encapsulated by lipid coating by analyzing their bifurcation structures as functions of driving pressure [15]. Qin et al. [16] explored the nonlinear dynamics of double moving bubbles in viscous liquid. Their research indicates that the interaction between bubbles strongly suppresses the pulsation of small bubble and slightly enhances the pulsation of large bubble. When the initial spacing between bubbles increases, the suppression effect becomes weak, and the nonlinear pulsations of bubbles are enhanced. Behnia et al. [12] studied the radius variation of a bubble driven by dual-frequency ultrasound. Bifurcation diagrams demonstrate that exerting high-frequency driving is beneficial for reducing the chaotic pulsation of bubble. The governing parameters in deciding pulsation are the frequency of high-frequency driving and the phase difference between the two driving. Moreover, they proposed a method to classify the nonlinear pulsation of bubble [13]. Research shows bifurcation pattern of bubble radius is closely related to the ratio of the bubble ambient radius to the wavelength of driving ultrasound. The systems having same ratio share significant similarities in the bifurcating behavior and can be classified to the same category. Zhang et al. [17] explored the nonlinear pulsations of double moving bubbles. In addition, they discussed the nonlinearity of secondary Bjerknes force with bifurcation diagrams. Research shows the translations of bubbles will enhance the nonlinearity and chaos of the secondary Bjerknes force. Dzaharudin et al. [18] investigated the influences of inter-bubble spacings and bubble sizes on the dynamical behavior of the bubble cluster. Their research reveals that if the microbubbles are clustered together, their pulsations are restricted, and the amplitudes of radii will be reduced. Increment of the driving acoustic power makes bifurcations and chaos of bubble radii emerge.

* Corresponding author.
E-mail address: wzchen@nju.edu.cn (W. Chen).

https://doi.org/10.1016/j.ultsonch.2022.106034
Received 31 March 2022; Received in revised form 1 May 2022; Accepted 9 May 2022
Available online 13 May 2022

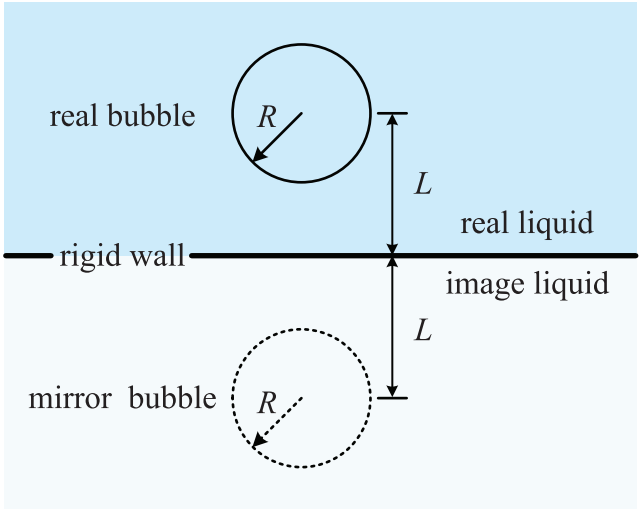

Fig. 1. Bubble near the rigid wall and its mirror image.

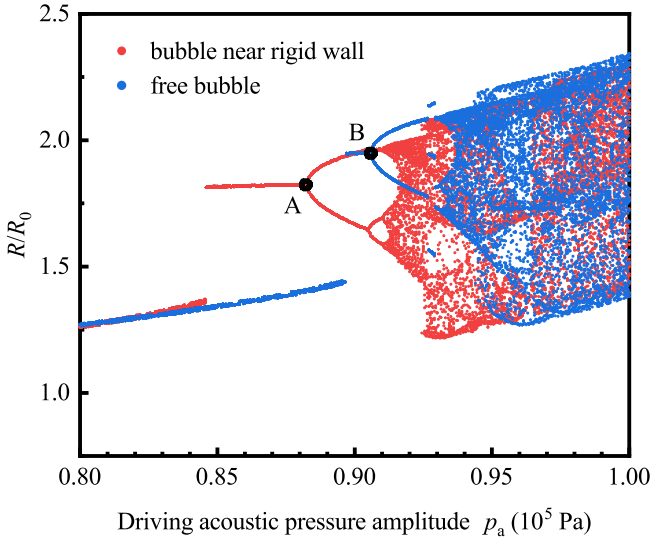

Fig. 2. Bifurcation diagram of R/R_0 for bubble near the rigid wall and free bubble.

Besides, it has been found that as the number of bubbles in the cluster increases, chaotic pulsation occurs at low ultrasonic power.

Although there exists several explorations about the nonlinearity of bubble pulsation, analysis on nonlinear pulsation of bubble near the wall with bifurcation diagram has not been reported. In real application, the bubble may be pulsating not far away from the rigid wall [19–22]. In this environment, influence of the boundary can not be ignored. This paper mainly discusses the nonlinear pulsation of the bubble near the rigid wall, and compares the dynamics of near-wall bubble with that of free bubble. The remainder of this article is organized as follows: In Section 2, the equation which describes the bubble pulsation affected by the rigid wall is introduced. In Section 3, the nonlinear pulsation of bubble closed to the rigid wall is analyzed with bifurcation diagrams and the other tools. Relations between the nonlinear pulsation and all kinds of parameters are introduced. Conclusions are summarized in Section 4.

2. Mathematical model of bubble near the rigid wall

Fig. 1 shows a bubble located in the liquid near the rigid wall. As that

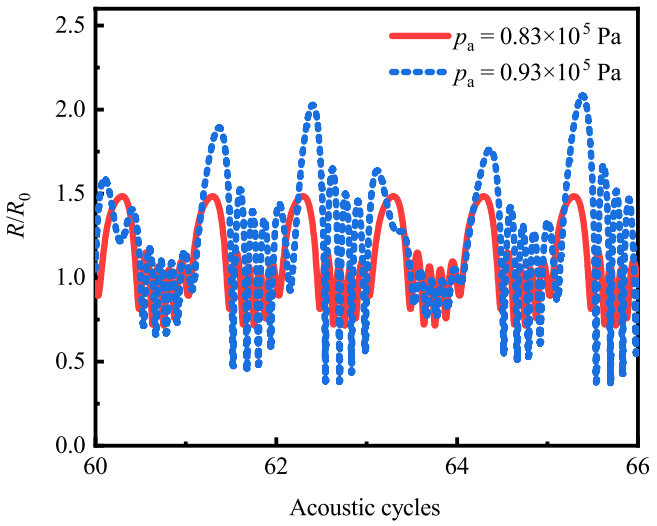

Fig. 3. Normalized radius of near-wall bubble driven by ultrasound of different acoustic pressure amplitudes.

in Refs. [23,24], the bubble is supposed to be spherical, and the shape instability of bubble is not considered. Besides, the translation of bubble is not taken into account. R is the radius of bubble, L is the distance between the bubble and the rigid wall. The rigid wall will reflect the acoustic wave radiated from the bubble. Influence of the rigid wall on a nearby bubble is equivalent to that of a mirror bubble in the image liquid. Properties of the image liquid are the same as that of the real liquid. The real bubble and the image bubble are the same size, and they are located symmetrically with respect to the rigid wall [23,24]. Therefore, radius of the mirror bubble is R, and the distance between the mirror bubble and the rigid wall is L.

Velocity potential produced by the mirror bubble is [4]

$$\varphi_{\mathrm{m}} = -\frac{R^2\dot{R}}{r}, \tag{1}$$

with r being the radial axis corresponding to the distance from the center of the mirror bubble. The overdot denotes the time derivative $\mathrm{d}/\mathrm{d}t$. In this research, distance between the real bubble and the mirror bubble is $2L$. So the radiation from the mirror bubble on the real bubble can be expressed as [25]

$$p_{\mathrm{rad}} = -\rho\dot{\varphi}_{\mathrm{m}} = \frac{\rho}{2L}\frac{\mathrm{d}\left(R^2\dot{R}\right)}{\mathrm{d}t}, \tag{2}$$

with ρ being the density of liquid. Radial pulsation of the bubble can be described by the well known Keller-Miksis equation [15,26]

$$\left(1-\frac{\dot{R}}{c}\right)R\ddot{R}+\left(\frac{3}{2}-\frac{\dot{R}}{2c}\right)\dot{R}^2=\frac{1}{\rho}\left(1+\frac{\dot{R}}{c}\right)p_x+\frac{R}{\rho c}\frac{\mathrm{d}}{\mathrm{d}t}p_x, \tag{3}$$

with c being the sound speed in the liquid. p_x can be expressed as [26]

$$p_x = p_{\mathrm{g}}-\frac{2\sigma}{R}-\frac{4\mu\dot{R}}{R}-\left(p_{\mathrm{ex}}+p_{\mathrm{rad}}\right)-P_0, \tag{4}$$

with σ being the surface tension, μ being the viscosity of liquid, P_0 being the atmospheric pressure, p_{ex} being the driving ultrasound pressure. In this publication, $p_{\mathrm{ex}} = -p_{\mathrm{a}}\sin(2\pi ft)$ with p_{a} being the amplitude of driving acoustic pressure. p_{g} is the pressure inside the bubble which can be calculated with [2]

$$p_{\mathrm{g}} = \left(P_0+\frac{2\sigma}{R_0}\right)\left(\frac{R_0^3-h^3}{R^3-h^3}\right)^{\gamma}, \tag{5}$$

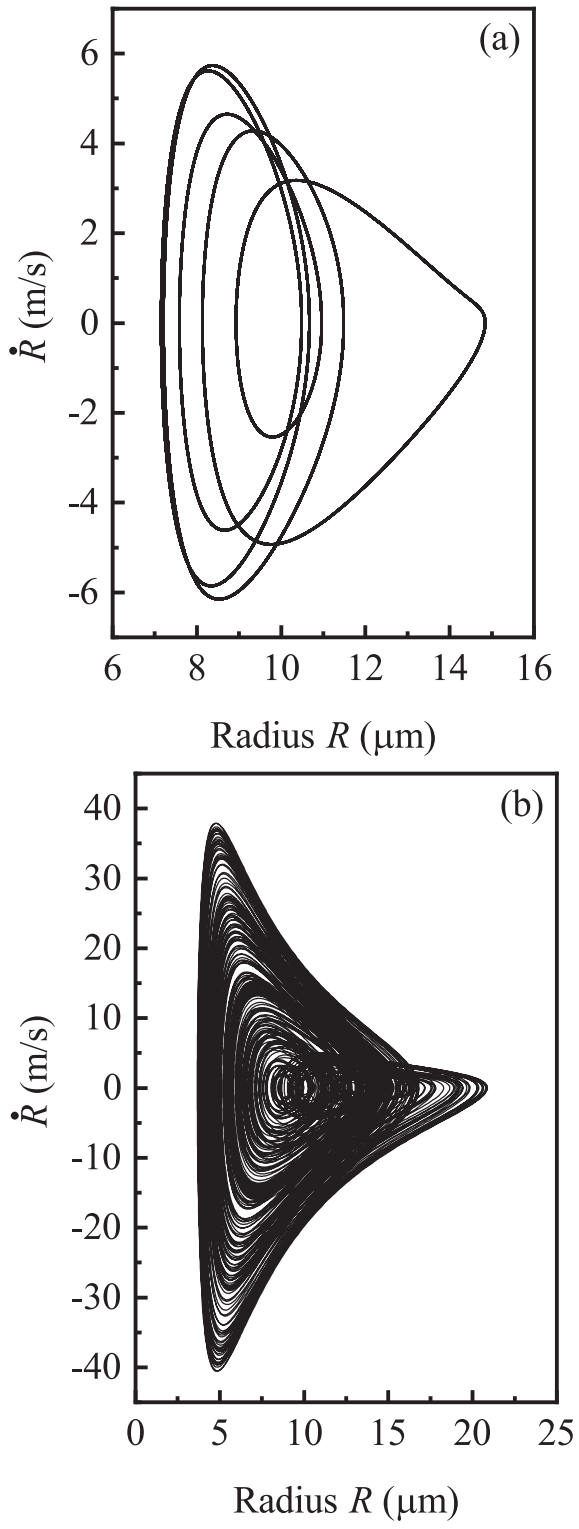

Fig. 4. Phase diagrams of near-wall bubble driven by ultrasound of different acoustic pressure amplitudes. (a) $p_a = 0.83 \times 10^5$ Pa, (b) $p_a = 0.93 \times 10^5$ Pa.

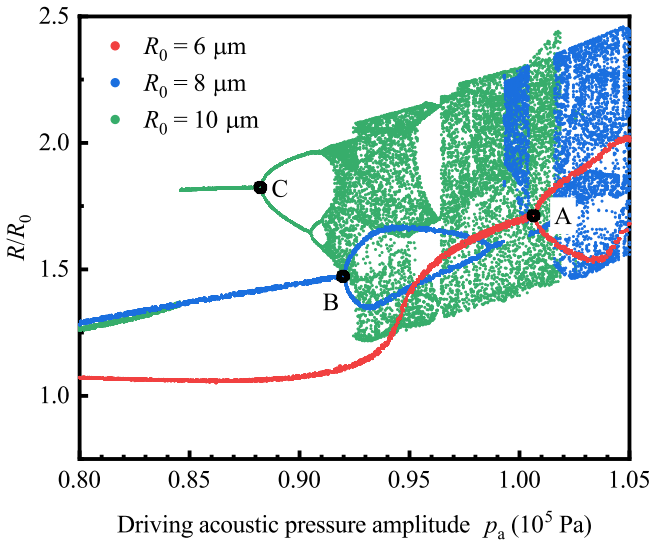

Fig. 5. Bifurcation diagram of R/R_0 for bubble near the rigid wall when the ambient radius takes different values.

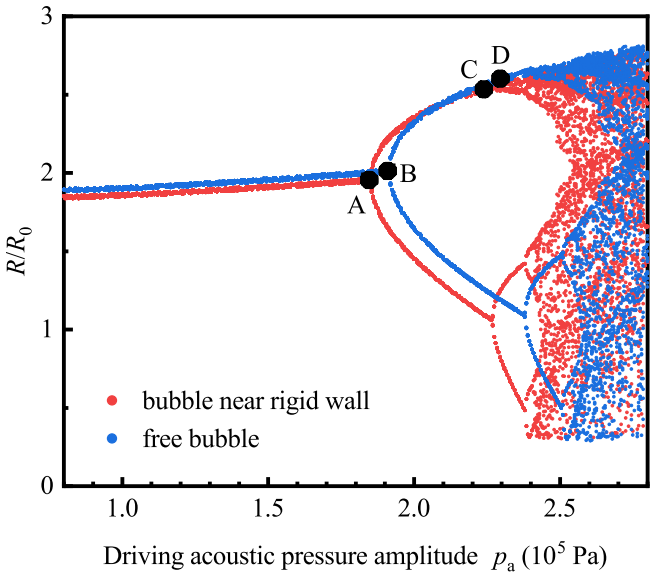

Fig. 6. Bifurcation diagram of R/R_0 for bubble near the rigid wall and free bubble.

with R_0 being the ambient radius of bubble, h being the hard-core radius which satisfies $h = \frac{R_0}{8.5}$. γ is the polytropic exponent of gas inside the bubble.

Neglecting high-order terms as suggested in Ref. [26], Eq. (3) can be modified to describe the pulsation of bubble near a rigid wall

$$\left(1-\frac{\dot{R}}{c}\right)R\ddot{R}+\left(\frac{3}{2}-\frac{\dot{R}}{2c}\right)\dot{R}^2=\frac{1}{\rho}\left(1+\frac{\dot{R}}{c}\right)p_s+\frac{R}{\rho c}\frac{\mathrm{d}}{\mathrm{d}t}p_s-\frac{1}{2L}\frac{\mathrm{d}\left(R^2\dot{R}\right)}{\mathrm{d}t}, \quad (6)$$

where p_s can be expressed as [26]

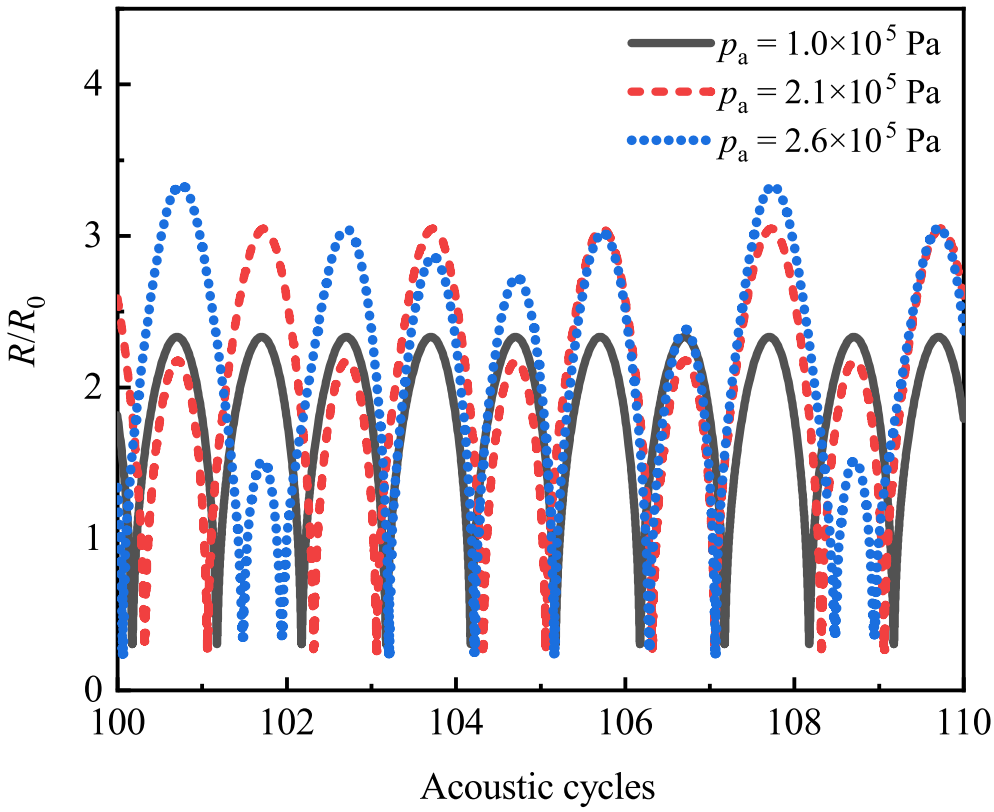

Fig. 7. Variation of R/R_0 for bubble driven by ultrasound of different amplitudes.

$$p_s = p_g - \frac{2\sigma}{R} - \frac{4\mu\dot{R}}{R} - p_{ex} - P_0. \tag{7}$$

3. Analysis on nonlinear pulsation of bubble

Radius of bubble near the rigid wall can be acquired by solving Eq. (6) with Runge-Kutta method. Radius of free bubble is calculated with Eq. (6) when $L\to\infty$. Parameters used in calculation are as follows: $P_0 = 1.013\times10^5$ Pa, $\rho = 998$ kg/m^3, $c = 1481$ m/s, $\sigma = 0.0725$ N/m, $\mu = 0.001$ Pa·s, $\gamma = 1.4$. Bifurcation diagrams are valuable in exploring the dynamics of nonlinear system over a wide range of control parameters [12,27,28]. In this paper, bifurcation diagrams are used as the primary tools for analyzing nonlinearity. As in Refs. [12–14,17], in each driving acoustic cycle, one point is stored for the illustration of bifurcation structure. In order to make sure that the dynamical state of bubble is stable, points are collected within 400 ~ 450 cycles. Dynamics of a bubble is closely related to the driving ultrasound and the properties of itself. In this section, influences of different factors on the nonlinearity of bubble pulsation will be introduced in details.

3.1. Relation with driving pressure amplitude

Setting $f = 60$ kHz, $R_0 = 10$ μm, $L = 100$ μm and do simulation. Fig. 2 shows bifurcation structures of the normalized bubble radius (R/R_0) versus driving acoustic pressure amplitude when the bubble is near the rigid wall or free. Point A and point B represent the beginnings of bifurcations for near-wall bubble and free bubble, respectively. If bifurcation does not appear, the bubble undergoes pulsation synchronized with driving. Pulsations in all cycles are identical. If there are two bifurcations, pulsations in two adjacent cycles are distinct, the period of bubble pulsation is twice the driving period. Chaos in bifurcation diagram means the pulsation is aperiodic. For both the near-wall bubble and the free bubble, as the driving acoustic pressure increases, double-bifurcation and chaos come out gradually. It is consistent with the contents in Refs. [15,27]. This phenomenon implies improving driving acoustic pressure will facilitate the nonlinear pulsation of bubble. Comparing the curves of bubbles under these two circumstances, it can be found the rigid wall makes the first bifurcation occur at low p_a (see point A). Similar phenomenon has been mentioned in Ref. [18]. In Ref. [18], additional bubbles cause the transition from non-bifurcation to double-bifurcation at low driving amplitude. In this research, influence of the rigid wall is equivalent to that of a mirror bubble. The performance mentioned above means the rigid wall enhances the nonlinear pulsation of nearby bubble. It could be because the acoustic wave radiated from bubble will be reflected by the rigid wall, and the reflected wave can be regraded as a perturbation on driving, which slightly improves its instability. As a result, unstable pulsation is easier to occur on bubble near the rigid wall rather than on free bubble.

Here the radius curves and the phase diagrams are used to illustrate the pulsation of near-wall bubble under different driving. Fig. 3 shows R/R_0 when p_a takes 0.83×10^5 Pa and 0.93×10^5 Pa, respectively. Under both driving, the bubble undergoes expansion and collapse several times in each acoustic cycle. When $p_a = 0.83\times10^5$ Pa, bifurcation does not appear (see Fig. 2), pulsations in all cycles are the same, and the pulsation period is the same as that of driving ultrasound (see solid line Fig. 3). But when $p_a = 0.93\times10^5$ Pa, chaos emerge in bifurcation diagram (see Fig. 2). Pulsations in different cycles are distinct (see dash line Fig. 3). Fig. 4(a) and (b) display the phase diagrams when p_a takes 0.83×10^5 Pa and 0.93×10^5 Pa, respectively. In Fig. 4(a), five circles can be seen. It is due to that the bubble undergoes five times of different pulsations in each driving cycle. In Fig. 4(b), there are lots of non-overlapping curves. This implies the bubble undergoes chaotic pulsation.

Fig. 5 shows the bifurcation structures of R/R_0 versus driving

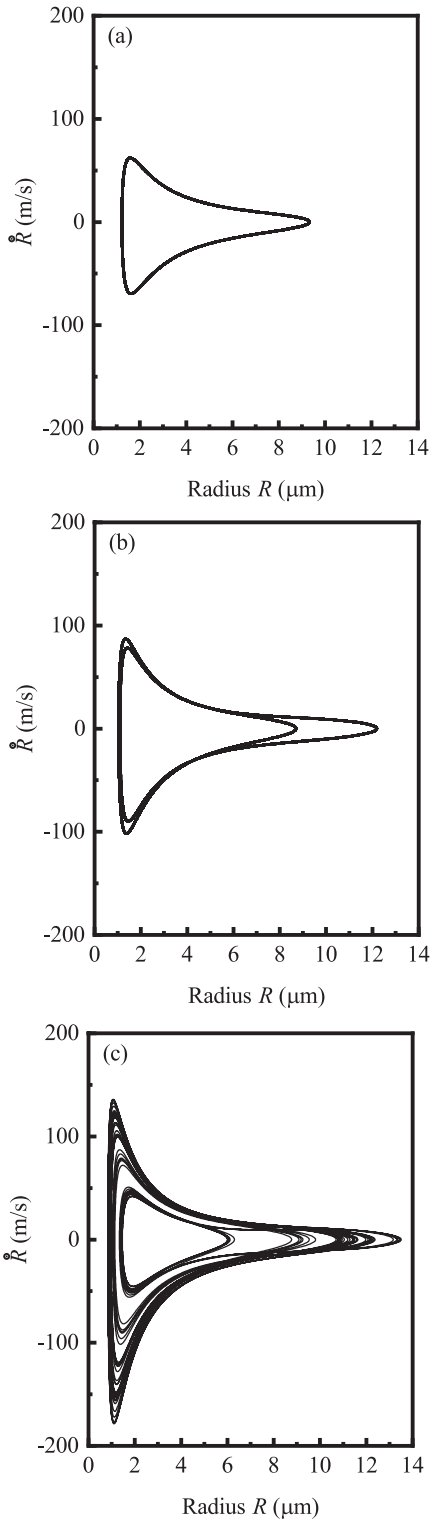

Fig. 8. Phase diagrams of bubble radius when the driving amplitude takes different values. (a) $p_a = 1.0 \times 10^5$ Pa, (b) $p_a = 2.1 \times 10^5$ Pa, (c) $p_a = 2.6 \times 10^5$ Pa.

acoustic pressure amplitude when the bubble is near the rigid wall. In calculation, $f = 60$ kHz and R_0 is set to be 6 μm, 8 μm and 10 μm, respectively. It can be found that with the growth of R_0, acoustic pressure amplitude corresponding to the first appearance of bifurcation decreases (see points A, B and C). Considering that low-amplitude driving is not conducive to the generation of nonlinear pulsation, from Fig. 5 it can be concluded nonlinear pulsation tends to become vigorous for bubble with large ambient radius.

Fig. 6 shows the bifurcation structures of R/R_0 as functions of driving pressure amplitude when the bubble is near the rigid wall (red dots) or free (blue dots). In simulation, $R_0 = 4$ μm, $f = 700$ kHz. In Fig. 6, points A and B correspond to the onsets of bifurcation for bubble near the rigid wall and the free bubble, respectively, and points C and D represent the onsets of chaos for bubble near the rigid wall and the free bubble, respectively. Bifurcation of bubble near the rigid wall emerges at low driving amplitude (see point A), and that of free bubble appears at high amplitude (see point B). Moreover, the rigid wall makes chaos emerge at low driving amplitude (see points C and D). Similar situations can be observed in Fig. 2 as well. That indicates the enhancement effect of rigid wall on the nonlinear pulsation of nearby bubble under high-frequency driving resembles that under low-frequency driving.

Fig. 7 and Fig. 8 are used for clearly demonstrating the pulsation details of bubble near the rigid wall under different driving. Values of R_0 and f are the same as that used in acquiring Fig. 6. Fig. 7 shows R/R_0 when p_a takes different values. When $p_a = 1.0 \times 10^5$ Pa, radius curves in all cycles are uniform. Under this condition, bifurcation does not appear (see Fig. 6). If $p_a = 2.1 \times 10^5$ Pa, radii in two adjacent acoustic cycles are different. The pulsation period is doubled, and two bifurcations can be found in Fig. 6. When $p_a = 2.6 \times 10^5$ Pa, variation of radius is aperiodic, chaos come out in bifurcation diagram (see Fig. 6). Fig. 8 shows the corresponding phase diagrams under various driving. In Fig. 8(a), only one closed curve can be seen. That means pulsations in all cycles are identical. Fig. 8(b) contains two closed curves, it is consistent with that the period is doubled (see Fig. 7) and two bifurcations of R/R_0 emerge (see Fig. 6). In Fig. 8(c), there are many non-overlapping curves. That means the pulsation of bubble is chaotic.

For further demonstrating the influence of rigid wall, Fig. 9 is used to show the driving acoustic pressures which correspond to the first appearances of bifurcation versus bubble-wall distance when $R_0 = 10$ μm, $f = 60$ kHz and $R_0 = 4$ μm, $f = 700$ kHz. The red solid line represents the pressure amplitude of initial bifurcation for free bubble when $R_0 = 10$ μm and $f = 60$ kHz, while the blue dash line represents the pressure amplitude of initial bifurcation for free bubble when $R_0 = 4$ μm and $f = 700$ kHz. Parameters of the free bubble are the same as that of the corresponding near-wall bubble. If the distance is promoted, bifurcation of R/R_0 begins at high driving acoustic pressure. Meanwhile, the slopes of curves decrease as distance grows. That indicates the impact of wall on the nearby bubble becomes weak as the bubble gets away. It can be inferred that if the distance becomes infinite, the pressure amplitude corresponding to the first emergence of bifurcation for near-wall bubble will be the same as that for free bubble.

3.2. Relation with ambient radius

Suppose $f = 60$ kHz, $p_a = 2.5 \times 10^5$ Pa, do simulation when the ambient radius R_0 increases from 3 μm to 6 μm. Bifurcation diagram of R/R_0 versus ambient radius for bubble near the rigid wall and the free bubble is shown in Fig. 10(a). Point A and point B correspond to the first

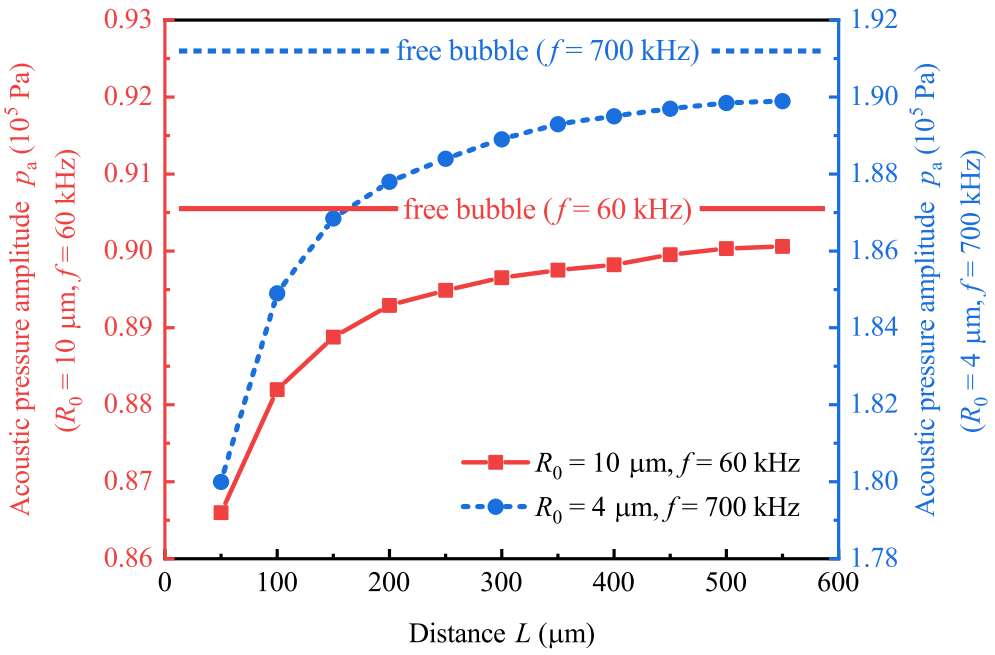

Fig. 9. Driving acoustic pressure amplitude corresponding to the first appearance of bifurcation versus bubble-wall distance.

appearances of bifurcations for near-wall bubble and free bubble, respectively. In Fig. 10(a), non-bifurcation and multi-bifurcation appear alternately with the rising of R_0, that implies synchronously pulsating with driving and pulsating with more than one period of driving happen by turns. Similar phenomenon has been observed in Refs. [17,29]. For bubble near the rigid wall, the first bifurcation appears at about $R_0 =$ 3.90 μm (see point A), and for free bubble, the first bifurcation appears when $R_0 = 4.20$ μm (see point B). When $f = 500$ kHz, bifurcation diagram of bubble near the rigid wall and free bubble is shown in Fig. 10(b). Meanings of points A and B are the same as that in Fig. 10(a). For these two types of bubbles, the curves come from non-bifurcation to double-bifurcation and then three-bifurcation gradually, and eventually become chaotic. The first bifurcation happens on $R_0 = 4.06$ μm for near-wall bubble (see point A) and on $R_0 = 4.28$ μm for free bubble (see point B). From Fig. 10, it can be easily found that no matter low-frequency or high-frequency driving is used, the bifurcation of R/R_0 appears at small ambient radius when the bubble is near the rigid wall (see points A in Fig. 10(a) and (b), and it appears at large ambient radius when the bubble is free (see points B in Fig. 10(a) and (b)). As previously mentioned, nonlinear pulsation is difficult to occur on bubble with small ambient radius, that means the rigid wall is beneficial for strengthening the nonlinear pulsation of nearby bubble.

Fig. 11 demonstrates the ambient radii corresponding to the first appearance of bifurcation versus bubble-wall distance when $f = 60$ kHz and $f = 500$ kHz. The dash line and the dot line represent the ambient radii corresponding to first bifurcation for free bubble when the driving frequencies are 60 kHz and 500 kHz, respectively. Under these two driving, as the distance increases, the first bifurcation emerges at large ambient radius of bubble. Besides, the slopes of curves in Fig. 11 decrease with the distance. That indicates the influence of the rigid wall diminishes if the distance increases.

3.3. Relation with driving frequency

In Refs. [13,29], bifurcation diagrams of bubble are plotted when driving frequency is swept in a range. For exploring the effect of driving frequency on nonlinearity, with the frequency-sweeping method referred in Refs. [13,29], we do simulation when $R_0 = 5$ μm, $p_a = 2.5 \times 10^5$ Pa and the driving frequency changes from 300 kHz to 850 kHz. It should be emphasized that some publications show the bubble is prone to be unstable if it becomes too large [30,31]. However, focus of this subsection is the shifts of driving frequencies corresponding to the beginnings of bifurcation and chaos. These frequencies are much lower than the resonant frequency, and strong pulsation will hardly happen. That means assuming the bubble remains spherical is reasonable. So as done in Refs. [13,29], the shape instability of bubble is not considered in frequency sweeping.

Fig. 12 shows the bifurcation structures of R/R_0 versus driving frequency for bubble near the rigid wall and free bubble. Points A and B represent the beginnings of bifurcation for near-wall bubble and free bubble, respectively. For bubble under these two circumstances, chaos emerge when the driving frequency locates around 700 kHz. According to the resonant frequency formula $f_0 = \frac{1}{2\pi R_0}\sqrt{\frac{3\gamma P_0}{\rho} + \frac{2(3\gamma-1)\sigma}{\rho R_0}}$ in Refs. [32,33], resonant frequency of a free bubble with ambient radius 5 μm is about 725 kHz (see the dash line in Fig. 12). That means around the resonant frequency, chaotic pulsation of bubble takes place. Comparing the chaotic regions of near-wall bubble and free bubble around the resonant frequency, it can be concluded the rigid wall makes the bifurcation and chaotic regions shift to low frequency. According to Ref. [24], the resonant frequency will be shifted downward under the impact of rigid wall. The shift of chaotic region in Fig. 12 may be attributed to the shift of resonant frequency. When $f > 800$ kHz, driving frequency is much larger than the resonant frequency of bubble, chaos will vanish gradually. In this scope, as driving frequency increases, nonlinearity of bubble pulsation decays.

Fig. 13 shows the driving frequency which corresponds to the first appearance of bifurcation in the band around resonant frequency versus the distance between bubble and the rigid wall. The dash line means the frequency of initial bifurcation for a free bubble (point B in Fig. 12). As the distance increases, the frequency corresponding to the initial bifurcation of near-wall bubble tends to be the same as that of free bubble. That may imply the influence of rigid wall on the shift of bubble resonant frequency decays if the bubble-wall distance becomes large.

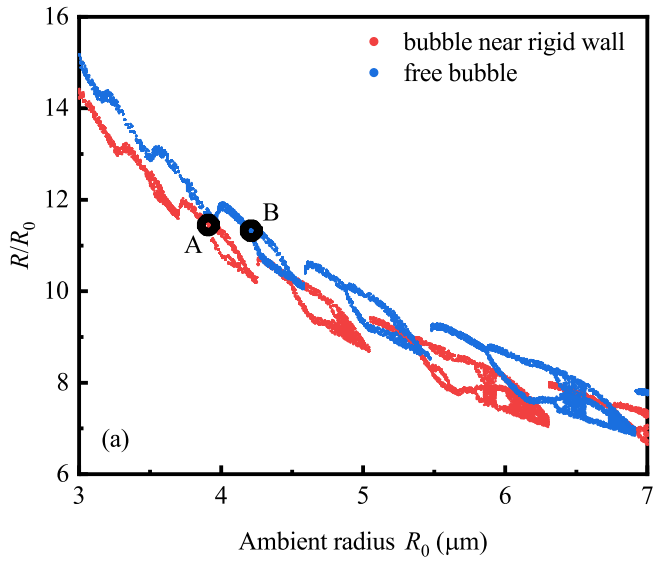

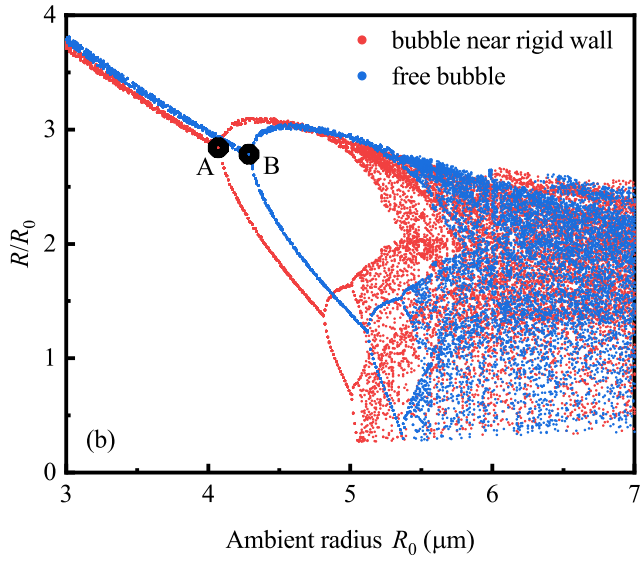

Fig. 10. Bifurcation diagrams of R/R_0 versus ambient radius for bubble near the rigid wall and free bubble. (a) $f = 60$ kHz, (b) $f = 500$ kHz.

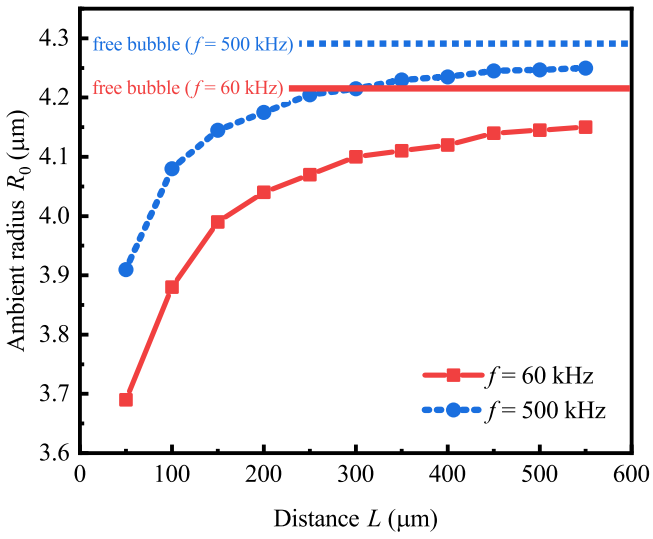

Fig. 11. Ambient radius corresponding to the first appearance of bifurcation versus bubble-wall distance.

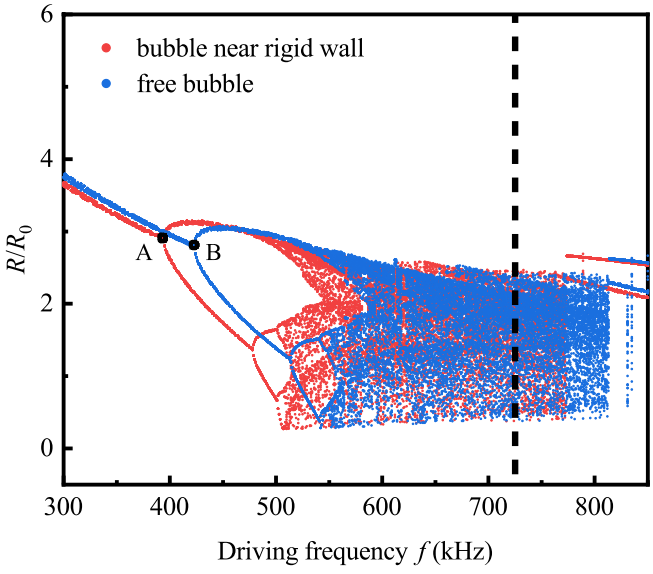

Fig. 12. Bifurcation diagram of R/R_0 versus driving frequency for bubble near the rigid wall and free bubble.

3.4. Relation with liquid viscosity

Liquid viscosity is an important factor in deciding bubble dynamics as well. In Refs. [16,17,29], bifurcation diagrams of bubble radii and secondary Bjerknes force versus viscosity are analyzed. In this paper, bifurcation structures of R/R_0 versus viscosity for near-wall bubble and free bubble when $p_a = 2.5 \times 10^5$ Pa, $R_0 = 5$ μm and $f = 600$ kHz are illustrated in Fig. 14. It should be noticed that in Fig. 14, viscosity in horizontal coordinate is decreasing. It is different from the other figures in this paper. For the bubble near the rigid wall as well as the free bubble, as the viscosity decreases, pulsations of bubbles change from non-bifurcation to multi-bifurcation, and then becomes chaos. It resembles the phenomena described in Refs. [16,29]. The above mentioned phenomenon means the viscosity of liquid will suppress the nonlinear pulsation of bubble. In Fig. 14, point A and point B represent the first appearances of bifurcation for near-wall bubble and free bubble, respectively. Comparing bifurcation structures of these two types of bubbles, it can be concluded that for bubble near the rigid wall, the first bifurcation appears at higher viscosity than that of free bubble. Considering high viscosity is disadvantageous for nonlinear pulsation, we can draw a conclusion that the rigid wall enhances the nonlinearity of bubble dynamics.

It is interesting that the shapes of bifurcation structures in Fig. 14 resemble that in Fig. 6. It is because for a bubble driven by ultrasound, improving diving pressure will overcome the viscous force which obstructs the bubble pulsation. To some extent, using host liquid with small viscosity is nearly equivalent to employing driving ultrasound with high acoustic pressure.

Fig. 15 shows the viscosity corresponding to the initial appearance of bifurcation for a near-wall bubble. The dash line represents that for a free bubble. If the distance becomes large, the viscosity for the near-wall bubble decreases to that for the free bubble gradually. It indicates the rigid wall enhances the nonlinearity as well.

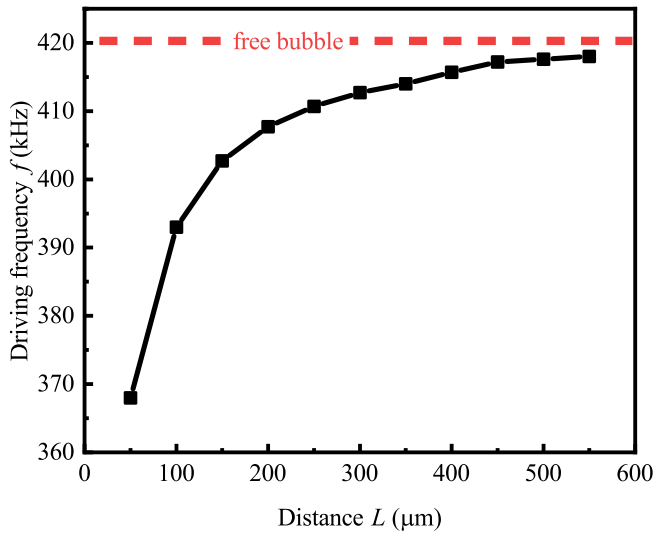

Fig. 13. Driving frequency corresponding to the first appearance of bifurcation versus bubble-wall distance.

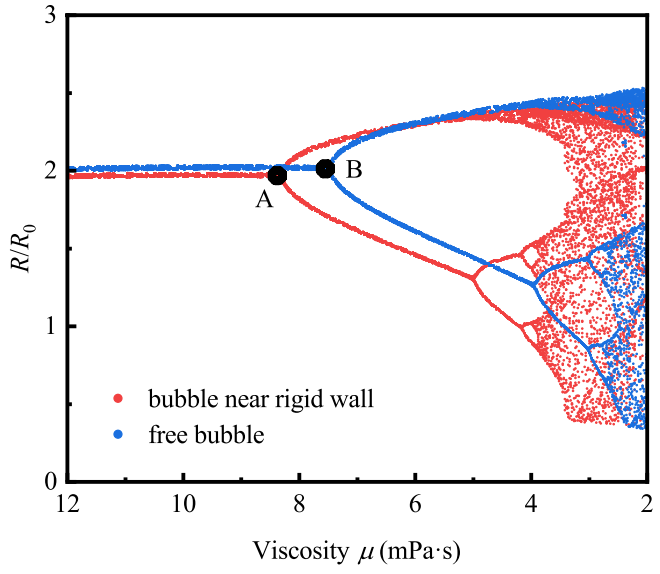

Fig. 14. Bifurcation diagram of R/R_0 versus liquid viscosity for bubble near the rigid wall and free bubble.

4. Conclusion

For a pulsating bubble near the rigid wall, the acoustic wave radiated from the bubble will be reflected by the rigid wall and exerts on the bubble itself. That makes the dynamics of near-wall bubble different from that of free bubble. In this paper, nonlinear pulsations of bubble near the rigid wall and free bubble are investigated and compared, and the influences of all kinds of factors are discussed in details. Investigations show the rigid wall makes the bifurcation and chaos appear at low driving acoustic amplitude and small bubble ambient radius, and makes the bifurcation disappear at high coefficient of viscosity. That

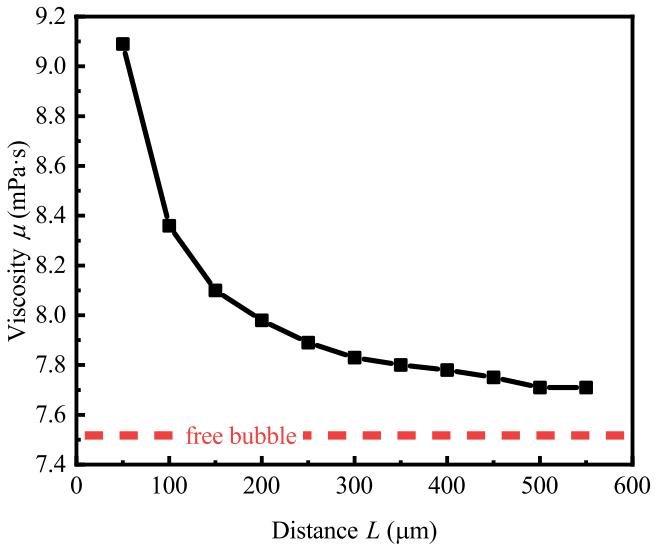

Fig. 15. Liquid viscosity corresponding to the first appearance of bifurcation versus bubble-wall distance.

means the rigid wall enhances the nonlinear pulsation of the nearby bubble. With the increasing of the spacing between the bubble and the wall, the driving pressure amplitude and the ambient radius corresponding to the initial bifurcation grow, and the viscosity corresponding to the initial bifurcation declines. That means the enhancement of the rigid wall on the nonlinearity of bubble pulsation falls down as the bubble moves away from the rigid wall. Investigation with frequency sweeping shows the driving frequency band corresponds to chaos around the resonant frequency of bubble will be shifted downward under the effect of rigid wall. This phenomenon may be attributed to the falling down of resonant frequency. In the future, influence of nonspherical pulsation on the nonlinearity will be studied, and the translation of bubble as well as the impacts of other bubbles will be considered. Besides, multi-frequency ultrasound will be used to drive the bubble. The relation between sonochemical reaction and nonlinearity is our future research objective as well.

CRediT authorship contribution statement

Xun Wang: Conceptualization, Methodology, Software, Writing – original draft. **Weizhong Chen:** Methodology, Funding acquisition, Supervision. **Min Zhou:** Writing – review & editing, Funding acquisition. **Zekun Zhang:** Writing – review & editing. **Lingling Zhang:** Writing – review & editing.

Declaration of Competing Interest

The authors declare that they have no known competing financial interests or personal relationships that could have appeared to influence the work reported in this paper.

Acknowledgments

This work was supported by the National Natural Science Foundation of China (Grant No. 12074185), Natural Science Basic Research Program of Shaanxi Province (Grant No. 2021JQ-655).

References

[1] N. Kerabchi, S. Merouani, O. Hamdaoui, Depth effect on the inertial collapse of cavitation bubble under ultrasound: Special emphasis on the role of the wave attenuation, Ultrason. Sonochem. 48 (2018) 136–150, https://doi.org/10.1016/j.ultsonch.2018.05.004.

[2] J. Liang, X. Wu, Y. Qiao, Dynamics of twin bubbles formed by ultrasonic cavitation in a liquid, Ultrason. Sonochem. 80 (2021), 105837, https://doi.org/10.1016/j.ultsonch.2021.105837.

[3] H. Gao, K. Pei, D. Lei, G. Hu, Y. Chao, A. Meng, H. Wang, W. Shentu, Ultrasonic cavitation in CO_2-expanded N, N-dimethylformamide (DMF), Ultrason. Sonochem. 78 (2021), 105713, https://doi.org/10.1016/j.ultsonch.2021.105713.

[4] Y. Shen, W. Chen, L. Zhang, Y. Wu, S. Kou, G. Zhao, The dynamics of cavitation bubbles in a sealed vessel, Ultrason. Sonochem. 82 (2022), 105865, https://doi.org/10.1016/j.ultsonch.2021.105865.

[5] S. Hong, G. Son, Numerical modelling of acoustic cavitation threshold in water with non-condensable bubble nuclei, Ultrason. Sonochem. 83 (2022), 105932, https://doi.org/10.1016/j.ultsonch.2022.105932.

[6] R. Pflieger, S.I. Nikitenko, M. Ashokkumar, Effect of NaCl salt on sonochemistry and sonoluminescence in aqueous solutions, Ultrason. Sonochem. 59 (2019), 104753, https://doi.org/10.1016/j.ultsonch.2019.104753.

[7] K. Nakajima, K. Noi, K. Yamaguchi, M. So, K. Ikenaka, H. Mochizuki, H. Ogi, Y. Goto, Optimized sonoreactor for accelerative amyloid-fibril assays through enhancement of primary nucleation and fragmentation, Ultrason. Sonochem. 73 (2021), 105508, https://doi.org/10.1016/j.ultsonch.2021.105508.

[8] K. Yasui, Numerical simulations for sonochemistry, Ultrason. Sonochem. 78 (2021), 105728, https://doi.org/10.1016/j.ultsonch.2021.105728.

[9] W. Tangsopa, J. Thongsri, Development of an industrial ultrasonic cleaning tank based on harmonic response analysis, Ultrasonics 91 (2019) 68–76, https://doi.org/10.1016/j.ultras.2018.07.013.

[10] R. Park, M. Choi, E.H. Park, W.J. Shon, H.Y. Kim, W. Kim, Comparing cleaning effects of gas and vapor bubbles in ultrasonic fields, Ultrason. Sonochem. 76 (2021), 105618, https://doi.org/10.1016/j.ultsonch.2021.105618.

[11] T. Yamamoto, R. Matsutaka, S.V. Komarov, High-speed imaging of ultrasonic emulsification using a water-gallium system, Ultrason. Sonochem. 71 (2021), 105387, https://doi.org/10.1016/j.ultsonch.2020.105387.

[12] S. Behnia, A.J. Sojahrood, W. Soltanpoor, O. Jahanbakhsh, Suppressing chaotic oscillations of a spherical cavitation bubble through applying a periodic perturbation, Ultrason. Sonochem. 16 (4) (2009) 502–511, https://doi.org/10.1016/j.ultsonch.2008.12.016.

[13] S. Behnia, A.J. Sojahrood, W. Soltanpoor, L. Sarkhosh, Towards classification of the bifurcation structure of a spherical cavitation bubble, Ultrasonics 49 (8) (2009) 605–610, https://doi.org/10.1016/j.ultras.2009.05.005.

[14] A.J. Sojahrood, D. Wegierak, H. Haghi, R. Karshfian, M.C. Kolios, A simple method to analyze the super-harmonic and ultra-harmonic behavior of the acoustically excited bubble oscillator, Ultrason. Sonochem. 54 (2019) 99–109, https://doi.org/10.1016/j.ultsonch.2019.02.010.

[15] A.J. Sojahrood, H. Haghi, R. Karshafian, M.C. Kolios, Nonlinear dynamics and bifurcation structure of ultrasonically excited lipid coated microbubbles, Ultrason. Sonochem. 72 (2021), 105405, https://doi.org/10.1016/j.ultsonch.2020.105405.

[16] D. Qin, Q. Zou, S. Lei, W. Wang, Z. Li, Nonlinear dynamics and acoustic emissions of interacting cavitation bubbles in viscoelastic tissues, Ultrason. Sonochem. 78 (2021), 105712, https://doi.org/10.1016/j.ultsonch.2021.105712.

[17] L. Zhang, W. Chen, Y. Shen, Y. Wu, G. Zhao, The nonlinear characteristics of the pulsations, translations and the secondary Bjerknes force, Chaos Soliton. Fract. 152 (2021), 111322, https://doi.org/10.1016/j.chaos.2021.111322.

[18] F. Dzaharudin, S.A. Suslov, R. Manasseh, A. Ooi, Effects of coupling, bubble size, and spatial arrangement on chaotic dynamics of microbubble cluster in ultrasonic fields, J. Acoust. Soc. Am. 134 (5) (2013) 3425–3434, https://doi.org/10.1121/1.4821202.

[19] L. Aired, A.A. Doinikov, A. Bouakaz, Effect of an elastic wall on the dynamics of an encapsulated microbubble: A simulation study, Ultrasonics 53 (1) (2013) 23–28, https://doi.org/10.1016/j.ultras.2012.03.008.

[20] M. Kauer, V. Belova-Magri, C. Cairós, H.J. Schreier, R. Mettin, Visualization and optimization of cavitation activity at a solid surface in high frequency ultrasound fields, Ultrason. Sonochem. 34 (2017) 474–483, https://doi.org/10.1016/j.ultsonch.2016.06.008.

[21] J. Ma, C.T. Hsiao, G.L. Chahine, Numerical study of acoustically driven bubble cloud dynamics near a rigid wall, Ultrason. Sonochem. 40 (2018) 944–954, https://doi.org/10.1016/j.ultsonch.2017.08.033.

[22] H. Wu, H. Zheng, Y. Li, C.D. Ohl, H. Yu, D. Li, Effects of surface tension on the dynamics of a single micro bubble near a rigid wall in an ultrasonic field, Ultrason. Sonochem. 78 (2021), 105735, https://doi.org/10.1016/j.ultsonch.2021.105735.

[23] M. Ida, T. Naoe, M. Futakawa, Direct observation and theoretical study of cavitation bubbles in liquid mercury, Phys. Rev. E 75 (2007), 046304, https://doi.org/10.1103/PhysRevE.75.046304.

[24] S.A. Suslov, A. Ooi, R. Manasseh, Nonlinear dynamic behavior of microscopic bubbles near a rigid wall, Phys. Rev. E 85 (2012), 066309, https://doi.org/10.1103/PhysRevE.85.066309.

[25] K.E. Morgan, J.S. Allen, P.A. Dayton, J.E. Chomas, A.L. Klibaov, K.W. Ferrara, Experimental and theoretical evaluation of microbubble behavior: effect of transmitted phase and bubble size, IEEE Trans. Ultrason. Ferr. 47 (6) (2000) 1494–1509, https://doi.org/10.1109/58.883539.

[26] M. Ida, T. Naoe, M. Futakawa, Suppression of cavitation inception by gas bubble injection: A numerical study focusing on bubble-bubble interaction, Phys. Rev. E 76 (2007), 046309, https://doi.org/10.1103/PhysRevE.76.046309.

[27] A.J. Sojahrood, H. Haghi, R. Karshafian, M.C. Kolios, Classification of the major nonlinear regimes of oscillations, oscillation properties, and mechanisms of wave energy dissipation in the nonlinear oscillations of coated and uncoated bubbles, Phys. Fluids 33 (2021), 016105, https://doi.org/10.1063/5.0032766.

[28] A.J. Sojahrood, H. Haghi, N.R. Shirazi, R. Karshafian, M.C. Kolios, On the threshold of 1/2 order subharmonic emissions in the oscillations of ultrasonically excited bubbles, Ultrasonics 112 (2021), 106363, https://doi.org/10.1016/j.ultras.2021.106363.

[29] S. Behnia, A. Jafari, W. Soltanpoor, O. Jahanbakhsh, Nonlinear transitions of a spherical cavitation bubble, Chaos Soliton. Fract. 41 (2) (2009) 818–828, https://doi.org/10.1016/j.chaos.2008.04.011.

[30] M.L. Calvisi, O. Lindau, J.R. Blake, A.J. Szeri, Shape stability and violent collapse of microbubbles in acoustic traveling waves, Phys. Fluids 19 (4) (2007), 047101, https://doi.org/10.1063/1.2716633.

[31] M. Versluis, D.E. Goertz, P. Palanchon, I.L. Heitman, S.M. van der Meer, B. Dollet, N. de Jong, D. Lohse, Microbubble shape oscillations excited through ultrasonic parametric driving, Phys. Rev. E 82 (2) (2010), 026321, https://doi.org/10.1103/PhysRevE.82.026321.

[32] A.A. Doinikov, Translational motion of a spherical bubble in an acoustic standing wave of high intensity, Phys. Fluids 14 (4) (2002) 1420–1425, https://doi.org/10.1063/1.1458597.

[33] X. Xi, F.B. Cegla, M. Lowe, A. Thiemann, T. Nowak, R. Mettin, F. Holsteyns, A. Lippert, Study on the bubble transport mechanism in an acoustic standing wave field, Ultrasonics 51 (8) (2011) 1014–1025, https://doi.org/10.1016/j.ultras.2011.05.018.